Dip-angle decomposition in relation with subsurface offset extended wave-equation migration

Raanan Dafni and William W. Symes, Rice University

Summary

Our proposal provides post-migration techniques for computing angle-domain common-image gathers (CIGs) from seismic images, extended by the subsurface offset, in relation with wave-equation migration methods. In addition to the commonly used decomposition of the scattering-angles, we associate the wave-equation migration with dip-domain image gathers as well. Our methodology suggests a system of Radon transform operators by introducing local transform relations between the subsurface offset image and the angle-domain components. The same subsurface offset extended image is employed to decompose scattering and dip angle CIGs individually, or to decompose a multi-angle CIG by showing simultaneously both angles on the gather's axis.
It is our belief that dip-angle information, decomposed by wave-equation migration, would have a great impact in making the scattering-angle reflection coefficient more reliable and noise-free, in addition to the expected acceleration of wave-equation inversion methods.

Introduction

Seismic depth migration in the angle-domain produces CIGs that collect energy from the seismic data which has been scattered over a specific angular direction. These gathers are referred here as Angle Domain CIGs (ADCIGs). One way to decompose ADCIGs in relation with wave-equation migration methods is by image space techniques, applied after the imaging condition (Rickett and Sava, 2002; Sava and Fomel, 2003; Biondi and Symes, 2004). They do not involve the original seismic data anymore, but the prestack image. Therefore, they are also considered as post-migration methods. The prestack image is usually the outcome of an extended imaging condition, which capture the image at different space or time correlation lags (i.e. subsurface offset or time shift) (Sava and Vasconcelos, 2011).
Angle-domain imaging involves two independent angle systems while computing ADCIGs: The scattering-angle system, and the dip-angle system (Koren and Ravve, 2011; Ravve and Koren, 2011). Due to their extensive use, tremendous effort was given throughout the years to study and compute scattering-angle ADCIGs (Jin et al., 2014). However, dip-angle ADCIGs decomposition in relation with wave-equation migration remained nearly unstudied.
In the following, we propose a set of image space techniques for the decomposing of ADCIGs in relation with subsurface offset extended image. We follow Sava and Fomel (2003) approach for calculating scattering-angle ADCIGs, and suggest complementary technique for dip-angle ADCIGs decomposition. It is shown that once scattering and dip dependent images are formulated, the derivation of a multi-angle ADCIG is within reach. This hybrid gather represents the image by both the scattering and dip angles, in the same fashion proposed by Dafni and Reshef (2012).

Subsurface offset relations with the angle-domain

Prestack migration operators can be described as the adjoint of extended Born-type modeling operators, after extending the definition of the reflectivity to depend on more degrees of freedom (Symes, 2008; Stolk et al., 2009). One conventional and natural choice to extend the reflectivity is by the horizontal subsurface offset. It is defined as the horizontal offset vector connecting the sunken shot and receiver in the subsurface, and involves an action at distance between the incident and scattered wavefields. The image $I(\mathbf{x},\mathbf{h})$, extended by the subsurface half-offset $\mathbf{h}$ takes the form

$$I(\mathbf{x},\mathbf{h}) = \int d\mathbf{x}_\mathbf{r} \int d\mathbf{x}_\mathbf{s} \int dt \frac{\partial^2}{\partial t^2} D(\mathbf{x}_\mathbf{r},t;\mathbf{x}_\mathbf{s}) \int d\tau G(\mathbf{x}+\mathbf{h},t-\tau;\mathbf{x}_\mathbf{r}) G(\mathbf{x}-\mathbf{h},\tau;\mathbf{x}_\mathbf{s}) \ , \qquad (1)$$

where $G(\mathbf{x},t)$ is the Green's function, $D(\mathbf{x}_\mathbf{r},t;\mathbf{x}_\mathbf{s})$ stands for the seismic data, and τ is the migration time (Stolk et al., 2009). In the 2D case, the subsurface offset becomes a scalar in equation 1.
In the angle domain, the reflectivity is a function of the direction of scattering. We follow Koren and Ravve (2011) and Ravve and Koren (2011) terminology, that employs the scattering-angle γ and the dip-angle ν to describe this direction in the 2D case.
Sava and Fomel (2003) linked between the subsurface offset and the scattering-angle, by involving local subsurface measurements associated with the interaction at a distance between the incident and scattered wavefields:

$$-\left.\frac{\partial z}{\partial h}\right|_{t,x} = \tan\gamma = -\frac{k_h}{k_z} \ . \qquad (2)$$

The left-hand-side implies that scattering-angles are associated with slope trajectories in the subsurface offset extended image space. The right-hand-side presents an equivalent relation, in Fourier domain, by the ratio between the subsurface offset and the vertical wavenumbers (k_h and k_z).
In this study, we introduce a complementary relation with regards to the dip-angles:

$$-\left.\frac{\partial z}{\partial x}\right|_{t,h} = \tan\nu = -\frac{k_x}{k_z} \ . \qquad (3)$$

The dip-angles are associated with slope trajectories, at constant h image sections, whereas in Fourier domain, they are associated with the ratio between the horizontal and vertical wavenumbers (k_x and k_z).

A suite of angle-domain decomposition techniques is formulated next according to equations 2 and 3. Scattering-angle and dip-angle ADCIGs are decomposed together with a hybrid multi-angle ADCIGs that depends simultaneously on both angles.

ADCIGs decomposition techniques

Scattering-angle ADCIGs are decomposed according to the relationship with the subsurface offset in equation 2. It includes the application of a classical Radon transform operator in the *z*-*h* domain, based on the angle-domain slope p=tanγ to guide the trajectory of integration. The Radon transform operator takes the form

$$A(x,z,p=\tan\gamma)=\int H(x,z+ph,h)dh \quad , \tag{4}$$

where A and H represents the angle and subsurface offset CIGs respectively. Sava and Fomel (2003) derived an equivalent expression in Fourier domain, which is more convenient for implementation, by a double Fourier transform over z and h axes (each transform is indicated by a tilde symbol):

$$\tilde{A}(x,k_z,p)=\tilde{\tilde{H}}(x,k_z,k_h) \quad , \tag{5}$$

where k_h=-pk_z is defined as the subsurface offset wavenumber. From equation 5 we conclude that 1D Fourier transforms of scattering-angle ADCIGs are equivalent to the 2D Fourier transforms of the subsurface offset extended image, subject to the stretch of the h axis according to the definition of k_h.

Dip-angle ADCIGs are decomposed according to the relationship with the subsurface offset in equation 3. As oppose to the scattering-angles, here the decomposition is derived across the subsurface offset CIGs. It includes the application of a classical Radon transform operator in the local *z*-*x* domain for individual h components, based on the angle-domain slope q=tanν to guide the trajectory of integration. The Radon transform operator takes the form

$$A(x,z,q=\tan\nu,h)=\frac{1}{\Delta x}\int_{-\Delta x/2}^{\Delta x/2} H(x+x',z+qx',h)dx' \quad , \tag{6}$$

The additional variable x' represents the locality of the transform around the x coordinate. Δx stands for the effective range where x' is sampled. Note that the decomposition is made for each subsurface offset independently as indicated by the additional fourth argument of the dip-angle ADCIG. We rewrite equation 6 in Fourier domain by a double Fourier transform over z and x' axes as follows:

$$\tilde{A}(x,k_z,q,h)=\frac{1}{2\pi}\mathrm{sinc}(k_x\Delta x)*\tilde{\tilde{H}}(k_x,k_z,h)e^{-ik_x x} \quad , \tag{7}$$

where k_x=-qk_z is defined as the horizontal wavenumber. The right-hand-side represents a convolution between a sinc function and the 2D Fourier transformed subsurface offset images multiplied by the exponential delay operator. Finally, the decomposition of the dip-angle ADCIGs is completed by a weighted averaging over all subsurface offsets, according to the weight function W_h that should be designed to peak around the zero subsurface offset:

$$\tilde{A}(x,k_z,q)=\frac{1}{2\pi}\sum_h W_h\,\mathrm{sinc}(k_x\Delta x)*\tilde{\tilde{H}}(k_x,k_z,h)e^{-ik_x x} \quad . \tag{8}$$

From equation 8 we conclude that 1D Fourier transforms of dip-angle ADCIGs are equivalent to the average of the convolutional 2D Fourier transformed subsurface offset extended images, subject to the stretch of the x axis according to the definition of k_x.

It is quite remarkable that the steps led to the dip-angle decomposition were made independent of the subsurface offset. As a result, the dip-angle ADCIG in equation 7 is still a function of the subsurface offset. Therefore, it can be further transformed to enable the additional decomposition of the scattering-angles. The final hybrid angle-domain CIG represents the image by the dip and the scattering angles simultaneously, and considered here as a multi-angle ADCIG. In relation with the classical Radon transform, the multi-angle ADCIG is decomposed by a double Radon transform operator of the form

$$A(x,z,q=\tan\nu,p=\tan\gamma)=\frac{1}{\Delta x}\int_{-\Delta x/2}^{\Delta x/2}\int H(x+x',z+qx'+ph,h)dhdx' \quad . \qquad (9)$$

The path of integration involves a plane, intersecting the subsurface offset extended image, defined by the angle domain slopes q and p. In Fourier domain, we recast equation 9 similarly to the two operators derived above, by a triple Fourier transform over z, x', and h axes as follows:

$$\tilde{A}(x,k_z,q,p)=\frac{1}{2\pi}\mathrm{sinc}(k_x\Delta x)*\tilde{\tilde{\tilde{H}}}(k_x,k_z,k_h)e^{-ik_x x} \quad . \qquad (10)$$

1D Fourier transforms of the multi-angle ADCIGs are equivalent to the convolutional 3D Fourier transforms of the subsurface offset extended image, subject to the stretch of x and h axis according to the definition of k_x and k_h.

Examples

We exemplify the proposed angle-domain decomposition techniques on a synthetic model, consisting of a single 10º dipping interface between two homogenous layers. The subsurface offset extended image was computed by a Born-type migration operator (Symes, 2008) as introduced in equation 1. True migration velocity was used for imaging. Figure 1a presents the resulting image by showing the zero subsurface offset image on the left, and one of the subsurface offset CIGs on the right (calculated at the position marked with the dashed line). A focused event is observed at the zero offset trace.

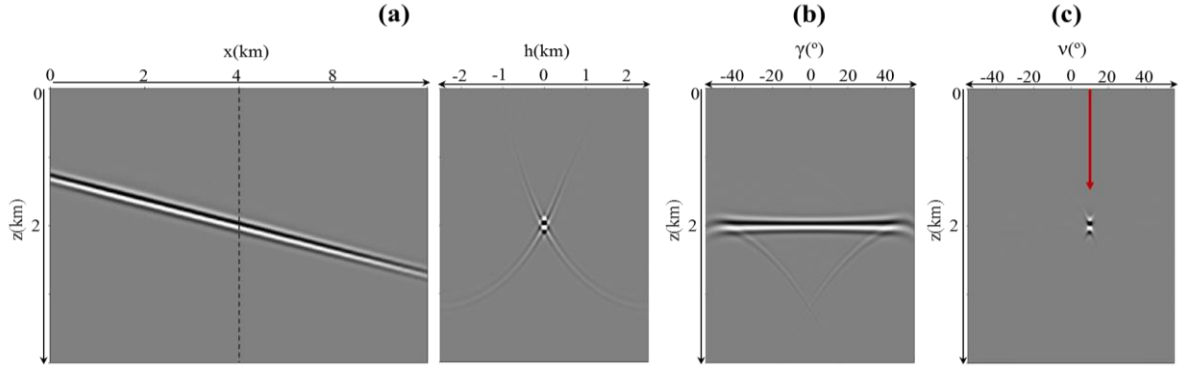

Figure 1 *Imaging of a 10º dipping reflector. (a) The subsurface offset extended image. Angle decomposition of (b) scattering-angle ADCIG, and (c) dip-angle ADCIG.*

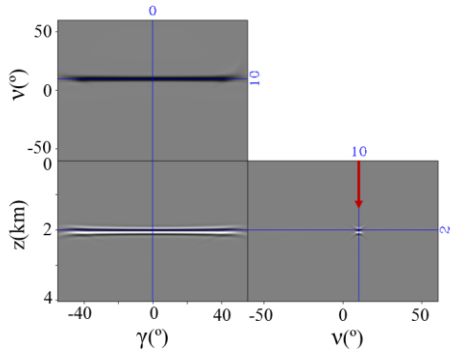

Figure 2 *Imaging of a 10º dipping reflector. Angle decomposition of multi-angle ADCIG (a 3D view).*

Scattering and dip angle ADCIGs are decomposed at the same marked position in Figures 1b and 1c respectively, according to equations 5 and 8. The scattering-angle ADCIG shows the typical flat appearance at the true depth of reflection (2km in this example). The reflectivity in the dip-angle ADCIG is prominently focused at the reflection depth. It indicates the specular dip-angle of reflection on the gather axis, as shown by the red arrow (10º in this example). This 'spot-like' response differs from the common 'smile-like' response many other dip-domain studies observe and report (Landa et al., 2008), although the same specular dip information is provided in both cases. We settle this contradiction by emphasizing that the dip-angle decomposition, proposed here, is a post-migration

technique. The tails of the 'smile'-like response were destructively lost through the migration in the subsurface offset domain, leaving only the stationary point of the smile prominent in the resulting image gather.
In Figure 2, the multi-angle ADCIG is decomposed according to equation 10. A 3D view is shown, by projecting the gather on its depth and angle axes. An intriguing image was revealed in the depth projection (top corner), extracted at the reflection depth of 2km. A coherent strip pattern is observed by combing the flat and the focused behavior of the image along the angle axes. All scattering-angles respond in-phase at the same specular dip-angle of 10º. This strip pattern has been introduced similarly by Dafni and Reshef (2012), although it was in the content of Kirchhoff migration methods.

Conclusions

We introduced angle-domain decomposition techniques for prestack wave-equation migration methods. A suite of Radon transform operators enables the calculation of scattering-angle, dip-angle and multi-angle ADCIGs from the post-migration subsurface offset extended image. A unique dip-domain response with regards to seismic reflections was discovered. A 'spot-like' (rather than a 'smile-like') event has been formed at the specular angle trace of the dip-angle ADCIG. It provides a focused in dip image, involving the specular contribution solely without the artificial tails.
We proposed a hybrid decomposition technique as well, where scattering and dip angles are decomposed simultaneously in the formulation of the multi-angle ADCIGs. When the true velocity model is known, the image point associated with a subsurface reflector shows a coherent strip pattern focused around the well-defined specular dip-angle. The decomposition of the dip-angles aside from the scattering-angles, as two sets of ADCIGs or as a single multi-angle ADCIG, increases the sensitivity to artifacts and noise while analyzing the post-migration image. Moreover, it might also assist to accelerate wave-equation inversion methods, such as full waveform inversion (FWI).

Acknowledgements

We are grateful to the sponsors of The Rice Inversion Project and Shell International Exploration and Production Inc. We also thank the Israeli Ministry of National Resources for partial financial support.

References

Biondi, B. and Symes, W. W [2004] Angle-domain common-image gathers for migration velocity analysis by wavefield-continuation imaging, *Geophysics*, **69**, no. 5, 1283-1298.
Dafni, R. and Reshef, M. [2012] Interval velocity analysis using multiparameter common image gathers, *Geophysics*, **77**, no. 4, U63-U72.
Jin, H., McMechan, G. A. and Guan, H. [2014] Comparison of methods for extracting ADCIGs from RTM, *Geophysics*, **79**, no. 3, S89-S103.
Koren, Z. and Ravve, I. [2011] Full-azimuth subsurface angle domain wavefield decomposition and imaging Part I: Directional and reflection image gathers, *Geophysics*, **76**, no.1, S1-S13.
Landa, E., Fomel, S. and Reshef, M. [2008] Separation, imaging and velocity analysis of seismic diffractions using migrated dip-angle gathers, 78th Annual Meeting, SEG, 2176-2180.
Ravve, I. and Koren, Z. [2011] Full-azimuth subsurface angle domain wavefield decomposition and imaging Part 2: Local angle domain, *Geophysics*, **76**, no.2, S51-S64.
Rickett, j. E. and Sava, P. C. [2002] Offset and angle-domain common image-point gathers for shot-profile migration, *Geophysics*, **67**, no. 3, 883-889.
Sava, P. C. and Fomel, S. [2003] Angle-domain common-image gathers by wavefield continuation methods, *Geophysics*, **68**, no. 3, 1065-1074.
Sava, P. C. and Vasconcelos, I. [2011] Extended imaging conditions for wave-equation migration, *Geophysical Prospecting*, **59**, no. 1, 35-55.
Stolk, C. C., de Hoop, M. V. and Symes, W. W. [2009] Kinematics of shot-geophone migration, *Geophysics*, **74**, no. 6, WCA19-WCA34.
Symes, W. W. [2008] Migration velocity analysis and waveform inversion, *Geophysical Prospecting*, **56**, no.6, 765-790.